PHYS 375 - Model of a Zero Age Main Sequence

Matthew Pereira Wilson – 20644035

DUE: April 10, 2018

---

1 Introduction

The Main Sequence stage of a star refers to the phase in stellar evolution when Hydrogen is being burnt in the stellar core. The project intends to use the equations of stellar structure to produce a working model of a Zero Age Main Sequence. The Zero Age classification of the modelled Main Sequence arises from the fact that the star's composition is assumed constant. This is only possible for stars that have initiated fusion very recently. The modelling was done by solving the equations of stellar structure for stars of different central temperature and calculating their surface conditions. The model results were tested against Luminosity-Mass and Radius-Mass empirical relationships from literature as well as empirical data from stars in open clusters. Individual stellar cases were also examined.

2 Equations of Stellar Structure

The differential equations solved for in the computation of each star are stated here for convenience. For an in depth description see Ryden chapters 14-15 [1].

The equations that describe stellar structure,

$$\frac{d\rho}{dr} = -\left[\frac{GM\rho}{r^2} + \frac{\partial P}{\partial T}\frac{dT}{dr}\right] \Big/ \frac{\partial P}{\partial \rho}, \tag{1}$$

$$\frac{dT}{dr} = -\min\left[\frac{3\kappa\rho L}{16\pi acT^3 r^2}, \left(1 - \frac{1}{\gamma}\right)\frac{T}{P}\frac{GM\rho}{r^2}\right], \tag{2}$$

$$\frac{dM}{dr} = 4\pi r^2 \rho, \tag{3}$$

$$\frac{dL}{dr} = 4\pi r^2 \rho \epsilon, \tag{4}$$

$$\frac{d\tau}{dr} = \kappa\rho. \tag{5}$$

From the combination of degenerate, ideal gas, and radiative pressures,

$$P(\rho, T) = \frac{(3\pi^2)^{2/3}}{5}\frac{h^2}{m_e}\left(\frac{\rho}{m_p}\right)^{5/3} + \frac{\rho kT}{\mu m_p} + \frac{1}{3}aT^4,$$

$$\text{where } \mu = [2X + 0.75Y + 0.5Z]^{-1},$$

we obtain,

$$\frac{\partial P}{\partial \rho} = \frac{(3\pi^2)^{2/3}}{3}\frac{h^2}{m_e m_p}\left(\frac{\rho}{m_p}\right)^{2/3} + \frac{kT}{\mu m_p},$$
$$\frac{\partial P}{\partial T} = \frac{\rho k}{\mu m_p} + \frac{4}{3}aT^3.$$

The energy reaction rates used were,

$$\epsilon_{PP} = 1.07 \times 10^{-7}\rho_5 X^2 T_6^4 \text{ W/kg},$$
$$\epsilon_{CNO} = 8.24 \times 10^{-26}\rho_5 X X_{CNO} T_6^{19.9} \text{ W/kg},$$
$$\epsilon(\rho, T) = \epsilon_{PP} + \epsilon_{CNO}.$$

Opacity was approximated to be,

$$\kappa(\rho, T) = \left[\frac{1}{\kappa_{H^-}} + \frac{1}{\max(\kappa_{es}, \kappa_{ff})}\right]^{-1}, \tag{6}$$

where,

$$\kappa_{es} = 0.02(1 + X),$$
$$\kappa_{ff} = 1.0 \times 10^{24}(Z + 0.0001)\rho_3^{0.7} T^{-3.5},$$
$$\kappa_{H^-} = 2.5 \times 10^{-32}\left(\frac{Z}{0.02}\right)\rho_5^{0.5} T^9.$$

Finally, the surface radius condition was defined to be,

$$\tau(\infty) - \tau(R_*) = \frac{2}{3}.$$

In addition to these equations, the model also required an end condition to stop the integration of the equations of stellar structure and a method for optimizing central density for a given central temperature. The end condition for the integration was defined as:

$$\delta\tau \equiv \frac{\kappa\rho^2}{|d\rho/dr|} \to 0.$$

$\delta\tau$ is an estimate of the remaining optical depth, and, in practice, if its value ever got lower than 1×10^{-3} the integration was stopped. The optimization condition for central density was the error between surface luminosity and the black body luminosity of the star,

$$f(\rho_c) = \frac{L_* - 4\pi\sigma R_*^2 T_*^4}{\sqrt{4\pi\sigma R_*^2 T_*^4 L_*}}. \tag{7}$$

Unfortunately, for high mass stars, the error function converges on a ρ_c value well before the black body luminosity. In these cases, the surface temperature was recalculated to match the luminosity of the star.

M(0)	0
L(0)	0
$\rho(0)$	ρ_c[1]
T(0)	T_c[2]

Table 1: Table of initial conditions for all stars.

The equations of stellar structure were solved with the initial conditions stated in table 1.

3 Project Code

The code requires a central temperature as its sole user input. It has a hard-coded range of central densities with which it attempts to find the correct central density for which the star's surface conditions are met. The correct central density corresponds to the root of equation 7 which was found numerically using the bisection method. The values of L_*, R_*, and T_* required for solving equation 7 were obtained by integrating the equations of stellar structure with Runge-Kutta-Fehlberg method (RKF45).

3.1 Bisection Method

The bisection method is a numerical tool for finding the root of a function. It requires that the function be continuous in the interval [a,b] and that it has opposite signs at the edges of the interval. The method can be simplified to the following steps:

1. Bisect the interval, $c = (a + b)/2$, ending up with two subsections [a,c]/[c,b]
2. Select which of the subsections holds the root. f (eq. 7) has opposite signs at the edges of the interval that holds the root.
3. Repeat until root is found or root is known to lie within a 1×10^{-12} interval

In our case, the bisection method was implemented with a Python *scipy.optimize* package. The initial solution interval [a,b] ranged from $0.3\,\mathrm{g/cm^3}$ to $500\,\mathrm{g/cm^3}$.

3.2 Runge-Kutta

The Runge-Kutta-Fehlberg method allows for the numerical solution of ordinary differential equations. The method computes both a 4th and 5th order result for each iteration. This allows for an error to be estimate on the 4th order solution. Table 2 provides the coefficients needed to recreate the RKF45 method.

The estimated error on the 4th order solution allows for the calculation of an *ideal step size*. This restrains the error in each iteration to be smaller than a certain value (h_{tol}). In turn, adaptive step size decreases computation time by increasing step size in areas of little

[1]Solved for with equation 7

[2]Input that determines the Main Sequence star

k_1	0					
k_2	1/4	1/4				
k_3	3/8	3/32	9/32			
k_4	12/13	1932/2197	-7200/2197	7296/2197		
k_5	1	429/216	-8	3680/513	-845/4104	
k_6	1/2	-8/27	2	-3544/2565	1859/4104	-11/40
z_{n+1}		16/135	0	6656/12825	-9/50	2/55
y_{n+1}		25/216	0	1408/2565	-1/5	0

Table 2: Butcher tableau for Runge-Kutta-Fehlberg's method [2]

sensitivity and increases accuracy by reducing step size in areas of high sensitivity. The ideal step size is given by,

$$h_{ideal} = \left(\frac{h_{tol}}{2|z_{n+1} - y_{n+1}|} \right)^{1/4}, \tag{8}$$

where z_{n+1} and y_{n+1} are respectively the 5th and 4th order solutions to the differential equation.

4 Main Sequence

The composition and adiabatic index of stars in the Main Sequence were assumed constant throughout each star. The values were based on the Sun and are shown in table 3.

Mass fraction of hydrogen	X	0.70
Mass fraction of helium	Y	0.28
Mass fraction of metals	Z	0.02
Adiabatic index	γ	5/3

Table 3: Constants used in generation of Main Sequence and individual stars.

4.1 Validation of Model

To ensure the model is working as intended, its output was tested against the Luminosity-Mass and Radius-Mass empirical relations from [1] as well as experimental data from [3]. The Luminosity-Mass and Radius-Mass relations are, respectively,

$$L/L_\odot = \begin{cases} 0.35(M/M_\odot)^{2.62} & M < 0.7M_\odot \\ 1.02(M/M_\odot)^{3.92} & M > 0.7M_\odot \end{cases} \tag{9}$$

$$R/R_\odot = \begin{cases} 1.06(M/M_\odot)^{0.945} & M < 1.66M_\odot \\ 1.33(M/M_\odot)^{0.555} & M > 1.66M_\odot. \end{cases} \tag{10}$$

The Luminosity-Mass and Radius-Mass relations are plotted against the model output in figures 1 and 2, respectively.

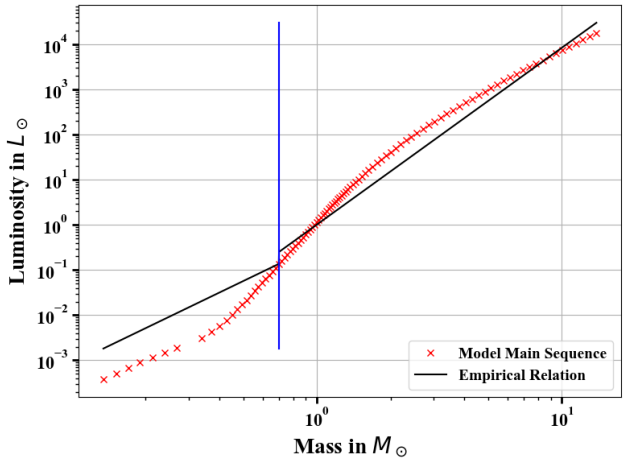

Figure 1: Luminosity-Mass relation

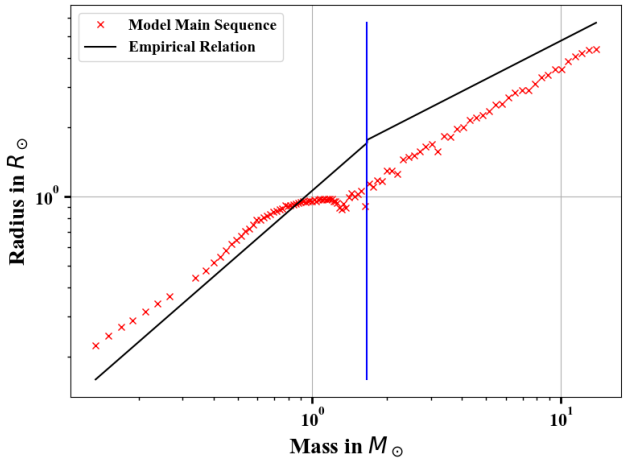

Figure 2: Radius-Mass relation

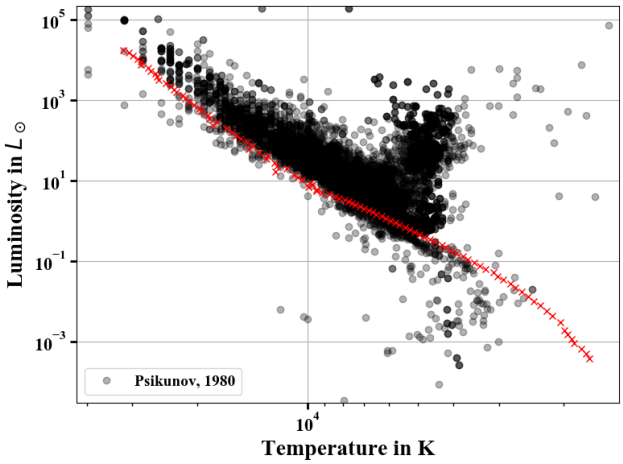

Figure 3: Hertzsprung-Russell diagram

Some discrepancies are clearly noticeable from the empirical relationships and the model output. With respect to figure 2, the model falls short of reproducing the Radius-Mass empirical relation around stars equal and bigger than the mass of the Sun ($1M_\odot$). This is likely due to two main reasons: the shift to a CNO dominated energy generation rate and the fact that the error function (equation 7) starts converging on a central density value well before the root is found. Assuming that the CNO energy generation rate is correct, this discrepancy may be attributed to approximations in the opacity (equation 6). As for the error function, further proof that this might be the cause for the discrepancy can be seen in figure 5. The mean relative error with respect to the empirical line ($\bar{\epsilon}$) decreases the more precise the bisection method is allowed to be. Though this isn't unexpected, it does show a trend. If precision was increase beyond 1e-12, the model's Radius-Mass relation should approach the empirical relation even further. From figure 1, the model also falls short of reproducing the Luminosity-Mass empirical relationship. In this case however, the shapes of the plots don't match and an increase in precision of the bisection method doesn't change that (see figure 4). This discrepancy could be attributed to the approximation in opacity, though other error sources should also be considered.

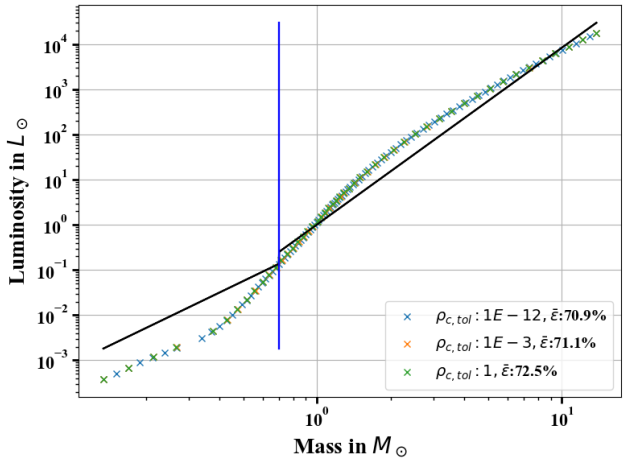

Figure 4: Luminosity-Mass relation

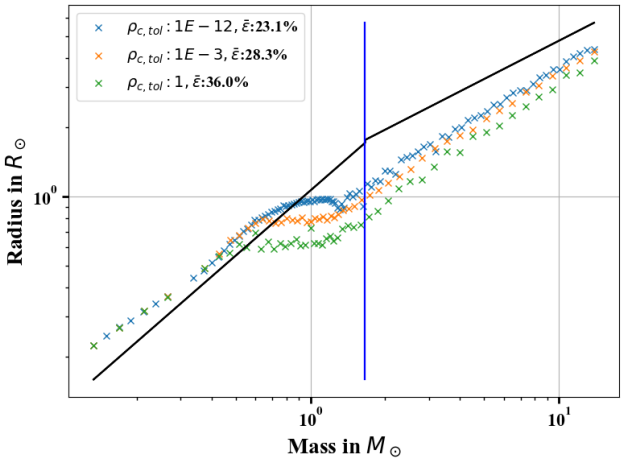

Figure 5: Radius-Mass relation

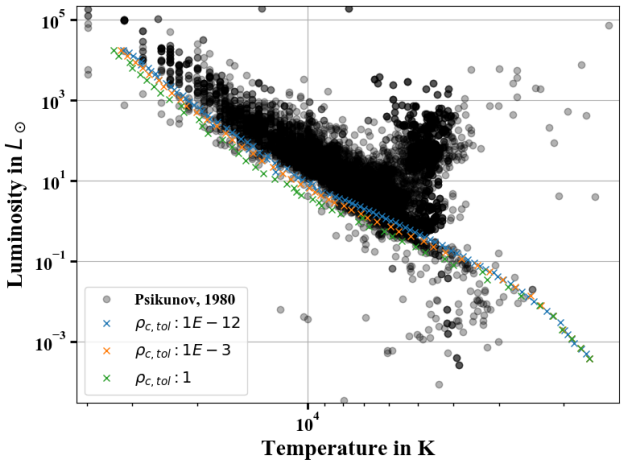

Figure 6: Hertzsprung-Russell diagram

Figure 3 and 6 show the Hertzsprung-Russell diagram of the model output as well as experimental data collected from open star clusters [3]. The model appears to match the experimental data fairly well. The shape of the model Main Sequence suggests the model is recreating the stellar structures correctly and the energy generation methods are dominant in their relevant regions. From figure 6, the increase in precision of the bisection method also leads to an increase in accuracy of the model.

The Hipparchus dataset [4] was also considered for validation of the model, but the color temperature approximation for effective temperature proved too coarse.

5 Individual Stars

To further study the structure of individual stars, two cases from the model were examined in detail. The stellar masses chosen for this were $0.5M_\odot$ and $4M_\odot$ because fusion generation rates in their cores are dominated by either proton-proton chain and CNO cycle, respectively. For all individual plots, the precision of the bisection method was left at 1×10^{-12}.

5.1 Low mass - $0.5M_\odot$

The model output for a $0.5M_\odot$ star is presented in table 4.

Central temperature	0.7×10^7 K
Mass	1.05×10^{30} kg
Luminosity	9.7×10^{24} W
Surface Temperature	2775 K
Radius	4.79×10^8 m

Table 4: Case study for a star dominated by PP chain

The stellar structure for the same mass star is shown in figure 7. Grey areas in the plots indicate that the region is unstable to convection, meaning that the main energy transport mechanism is convection. These convective zones were identified by the condition dlogP/dlogT equal to 2.5. The transition region between the convective and radiation zones, also known as tachocline, is visible in the temperature plot of the top left graph of figure 7. At this boundary, the temperature plot shows an inflection in slope caused by the switch in energy transport mechanisms.

When talking about convection/radiation zones, it is important to remember that the system will always try to have the smallest temperature gradient possible! This means it will choose the most efficient energy transfer mechanism under those conditions. The convective zones near the surface of the star, in either low or high mass stars, are usually caused by the region's relatively low temperature. The low temperature allows for the formation and existence of some atomic hydrogen. Atomic hydrogen increases the heat capacity of the medium and its opacity. From equation 3, we see how the radiation temperature gradient is directly proportional to opacity, so it starts to becomes beneficial for the system to use convection as the energy transport mechanism. Evidence for the increase in opacity at the surface comes from the middle right graph in figure 7. Additionally, the formation of atomic hydrogen increases the heat capacity of the medium, which increases the amount of energy that convection can move, further benefiting convection as the energy transport mechanism.

The dominant energy generation source for stars with masses smaller than $1M_\odot$ is the proton-proton chain. The evidence for this comes from the dL/dr graph in figure 7 (middle left), where the total change in luminosity corresponds almost entirely to the change in luminosity by the proton-proton chain.

The dominant opacity for most of the star's radius is caused by free-free interactions. The exception to this is a very shallow region on the surface of the star when the temperature gets low enough for H^- to form, at which point H^- interactions become the dominant factor for opacity. See figure 7 (middle right) for the stellar model output for opacity.

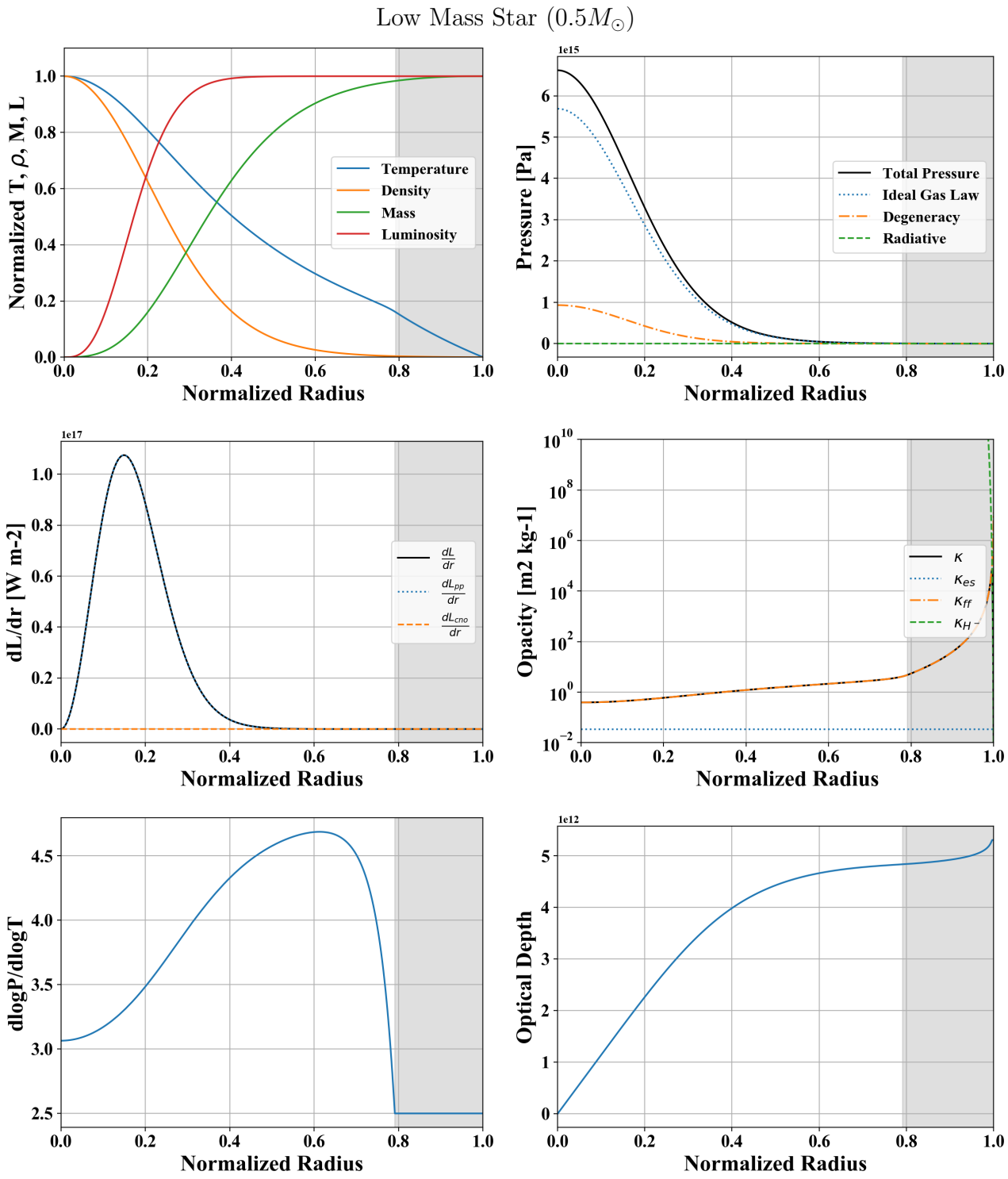

Figure 7: Top left: Normalized values of temperature, density, mass, and luminosity. Top right: Pressure and its different components. Middle left: Change in luminosity and its different components. Middle right: Log plot of opacity and its different components. Bottom left: Plot of dlogP/dlogT. When the value of dlogP/dlogT is equal to 2.5 the area is unstable to convection. Bottom right: Optical depth of star beginning from center of star.

5.2 High mass - $4M_\odot$

The surface conditions outputted from the model for a $4M_\odot$ star are presented in table 5. The stellar structure for the same mass star is shown in figure 8.

Central temperature	2.45×10^7 K
Mass	7.96×10^{30} kg
Luminosity	1.9×10^{29} W
Surface Temperature[3]	19 700 K
Radius	1.33×10^9 m

Table 5: Case study for a star dominated by CNO chain

This high mass star has two convective zones, as calculated by dlogP/dlogT plot of figure 8 (bottom left). The convective zone near the surface is caused by the same increase in the radiative temperature gradient due to the increase in opacity. However, the new convective zone at the core of the high mass star is caused by the high temperature dependence of the CNO cycle, which is $\propto T^{19.9}$.

The dominant energy generation source for stars with masses larger than $1M_\odot$ is the CNO cycle. The evidence for this comes from the dL/dr graph in figure 8, where the total change in luminosity corresponds almost entirely to the change in luminosity by the CNO cycle. The high temperature dependence of the energy generation rate drives the instability of the convective region.

The star's opacity is dominated by different factors in different regions. For about half of the star's radius, starting from the core, the opacity of the star is dominated by a flat electron scattering. After that, free-free opacity becomes the dominant factor until the surface. Realistically, since the surface of this star is above 10 000 K, we don't expect atomic hydrogen to exist, much less κ_{H^-} to be significant.

[3]Corrected surface temperature to match the star's black body luminosity

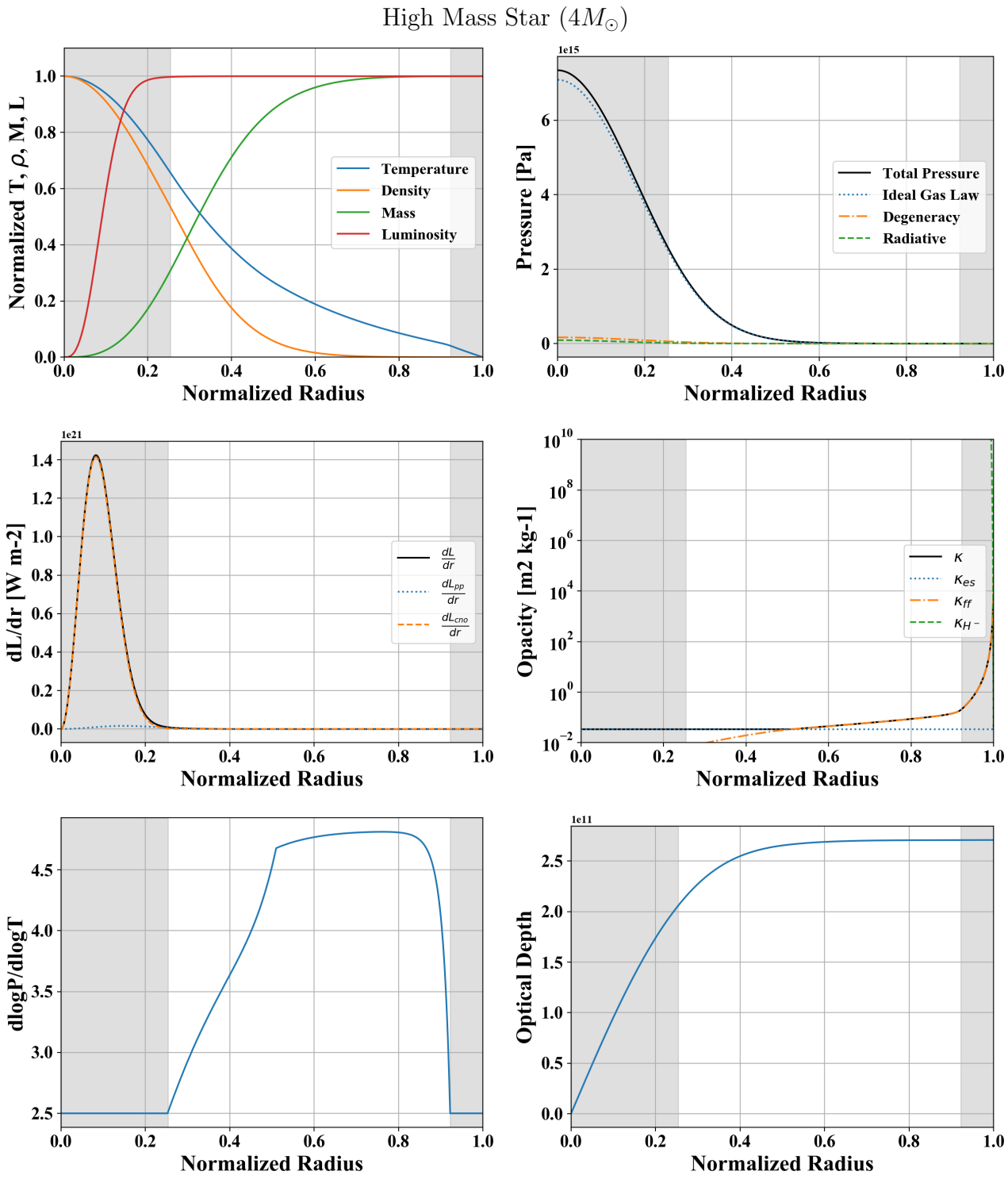

Figure 8: Top left: Normalized values of temperature, density, mass, and luminosity. Top right: Pressure and its different components. Middle left: Change in luminosity and its different components. Middle right: Log plot of opacity and its different components. Bottom left: Plot of dlogP/dlogT. When the value of dlogP/dlogT is equal to 2.5 the area is unstable to convection. Bottom right: Optical depth of star beginning from center of star.

5.3 Comparison of Stellar Cases

There are a few differences between the stellar structure of high and low mass stars.

- Both stellar cases have convective zones at the surface, though only the high mass star has a convective core
- The high mass star's energy generation rate is dominated by the CNO cycle while the low mass star's is dominated by the PP chain
- Free-free opacity is common to both stellar cases, though it is much more prevalent in the low mass case. The high mass star's opacity is also caused electron-scattering for a large inner region. The low mass star had a shallow optically thick layer at the surface caused by H^- photo-ionization
- The low mass star shows a relatively high dependency on degeneracy pressure. Pressure in both stars is mostly comprised of ideal gas pressure

6 Conclusion

The equations of stellar structure were successfully solved to recreate a Zero Age Main Sequence. The model output was tested against Luminosity-Mass and Radius-Mass empirical relations and showed some discrepancies. This discrepancy is explained by the precision limit in the bisection function. This could have been circumvented with the implementation of our own bisection function that allowed for double or long double precision. The model was also validated against experimental data from stellar clusters, which it recreated reasonably well.

The model recreated the structure of a low mass ($0.5M_\odot$) and a high mass stars ($4M_\odot$). The convection zones, dominant energy generation rates and opacity were correctly modeled for both stars. The two stellar structure were compared and their differences identified.

References

[1] Ryden B. and Peterson B., *Foundations of Astrophysics*, San Francisco (CA): Pearson Education. 2009.

[2] Mathews, J. and Fink K., *Numerical Methods Using MATLAB* 4th Edition, Upper Saddle River (NJ): Prentice-Hall Inc. 2004. ISBN: 0-13-065248-2

[3] Piskunov A.E., *Masses and Ages of Stars in 68 Open Clusters*, Bulletin d'Information du Centre de Donnees Stellaires, Vol. 19, p. 67-70. 1980.

[4] ESA 1997, *The Hipparcos and Tycho Catalogues*, http://cdsarc.u-strasbg.fr/viz-bin/Cat?, Last access: 10 Apr 2018.